Astron. Nachr. / AN **337**, No. 10, 1024 – 1032 (2016) / **DOI** 10.1002/asna.201612428

Observations of solar X-ray and EUV jets and their related phenomena

D. E. Innes[1,2,⋆], **R. Bučík**[1,3], **L.-J. Guo**[1,2], and **N. Nitta**[4]

[1] Max-Planck-Institut für Sonnensystemforschung, 37077 Göttingen, Germany
[2] Max Planck/Princeton Center for Plasma Physics, Princeton, NJ 08540, USA
[3] Institut für Astrophysik, Georg-August-Universität Göttingen, D-37077 Göttingen, Germany
[4] Lockheed Martin Advanced Technology Center, Palo Alto, CA 94304, USA

Received 2016 Aug 31, accepted 2016 Sep 02
Published online 2016 Dec 02

Key words Sun: activity – Sun: magnetic field – Sun: particle emission – Sun: X-rays

Solar jets are fast-moving, elongated brightenings related to ejections seen in both images and spectra on all scales from barely visible chromospheric jets to coronal jets extending up to a few solar radii. The largest, most powerful jets are the source of type III radio bursts, energetic electrons and ions with greatly enhanced ^{3}He and heavy element abundances. The frequent coronal jets from polar and equatorial coronal holes may contribute to the solar wind. The primary acceleration mechanism for all jets is believed to be release of magnetic stress via reconnection; however the energy buildup depends on the jets' source environment. In this review, we discuss how certain features of X-ray and EUV jets, such as their repetition rate and association with radio emission, depends on their underlying photospheric field configurations (active regions, polar and equatorial coronal holes, and quiet Sun).

1 Introduction

Jets are transient, collimated and fast with respect to the thermal speed of the plasma in the jet. They are seen with innumerable different forms, scales and spectral signatures on the Sun. Here we focus on X-ray (Cirtain et al. 2007; Shibata et al. 1992; Shimojo et al. 1998) and extreme ultraviolet (EUV) jets (Alexander & Fletcher 1999; Nisticò et al. 2009) and their associations with cold plasma surges (Chae et al. 1999), filaments (Sterling et al. 2015), and solar energetic particles (SEPs) (Nitta et al. 2015; Wang et al. 2006b). The consensus is that all solar jets result from magnetic reconnection and that the jet energy and characteristics depend on the magnetic environment and energy buildup process at the jet source. The aim of this review is to provide a overview of the different types of jets from an observational point-of-view. For example, what is the difference between jets caused by the motion of sunspot satellite flux (Canfield et al. 1996), flux emergence (Cheung et al. 2015), and those resulting from the winding up of fields surrounding minority flux in coronal holes (Guo et al. 2013; Schmieder et al. 2013)? How do these compare with eruptions in the quiet Sun (Innes et al. 2009) or along coronal hole boundaries (Madjarska et al. 2004)?

There are many types of jets and the boundaries between different categories are not well-defined. Here we separate jets into two main types: interplanetary and coronal. The interplanetary jets are associated with sub-relativistic electron beams detected by decametric-hectometric (D-H) type III radio bursts and, depending on the magnetic connectivity of the source, SEPs. These are strong jets associated with a sufficiently high flux of energetic particles for them to produce a type III radio burst. They come from open field regions so that the accelerated particles can propagate into interplanetary space. Those jets seen extending into the corona in X-ray or EUV images but without producing D-H type III's are categorised as coronal. Either they are strong jets but SEPs are ejected along closed field so return to the Sun, or they are not powerful enough to produce a sufficient flux of sub-relativistic electrons to create a type III.

There are many discussions of jets in the literature. The first surveys of X-ray jets were based on Yohkoh observations (Shimojo et al. 1996, 1998; Tsuneta et al. 1991). Here the jets were sorted according to the underlying magnetic field. Most jets (72 %) came from mixed polarity regions near pores or sunspots and 20 % came from unipolar or plage regions near active regions with and without minor polarity flux concentrations.

Originally, X-ray jets were thought to be caused by flux emergence and subsequent reconnection with open magnetic flux (Shibata et al. 1992). Later it was observed that X-ray jets may be associated with moving magnetic features (MMFs) and co-temporal and spatial with spinning Hα surges (Canfield et al. 1996), suggesting that reconnection between the flux constraining twisted Hα filament plasma, rather than emerging flux, and adjacent open flux was the cause of the jets. One of the questions addressed by our survey is how long after flux emergence are EUV and X-ray jets seen. Many papers report a significant delay between jet formation and flux emergence in contrast to recent 3D

⋆ Corresponding author: innes@mps.mpg.de

simulations of flux emergence into open field regions that predict jets at the time of flux emergence (Moreno-Insertis & Galsgaard 2013; Moreno-Insertis et al. 2008).

Early observations of X-ray jets associated with bursts of metric radio emission implied that the jet mechanism was able to accelerate sub-relativistic electrons along dense corona structures (Aurass et al. 1994; Kundu et al. 1995; Raulin et al. 1996). Further confirmation came from observations of jets which were co-incident with hard X-rays from their footpoints (Chen et al. 2013; Krucker et al. 2011; Nitta 1997; Nitta et al. 2008) and from the jet itself (Bain & Fletcher 2009; Glesener et al. 2012).

With the launch of Hinode (Kosugi et al. 2007), fainter X-ray jets in polar and equatorial coronal hole regions could be investigated (Cirtain et al. 2007; Raouafi et al. 2010; Subramanian et al. 2008). Török et al. (2009) proposed that coronal hole jets occur when a small concentration of minor polarity flux emerges in a coronal hole creating an anemone-shaped system of loops centered on the minor polarity. When the system is twisted about the central axis, stress builds up that can be explosively released, driving high-speed jets.

Another agent is believed to cause jets along the boundaries of large coronal holes. The open flux, rooted in the coronal holes, extends far into the corona where it rigidly co-rotates. But the underlying photospheric regions differentially rotate. The different speeds force the flux at coronal hole boundaries to continuously readjust and reconnect (Kahler & Hudson 2002; Wang & Sheeley 1993), producing jets (Madjarska et al. 2004).

Jets have also been seen from junctions of supergranular cells where vortices entrain mixed polarity flux creating conditions for small eruptions and jets (Attie et al. 2016; Innes et al. 2009; Innes & Teriaca 2013).

Table 1 categorises jets recently reported in the literature. One criterion for inclusion in the table is that the jet was observed after 1994 when WIND/WAVES (Bougeret et al. 1995) data are available so that they can be identified as interplanetary (IP) or coronal (C). We also chose those jets with co-temporal and spatial photospheric magnetic field data, and for completeness a few publications reporting features of polar or limb jets. Column 1 gives the jet type and in brackets the source environment: SS – sunspot; MMF - moving magnetic features on the outer edge of sunspot penumbra; Plage – plage; ARCH - active region coronal hole; PCH – polar coronal hole; ECH – equatorial coronal hole with quiet Sun field strengths; QS – quiet Sun. Column 2 gives the type of SEPs, if any, associated with the jet. All ^{3}He jets were also associated with 40–100 keV electrons and 0.4–1 MeV nucleon^{-1} ions. Column 3 gives the time in hours between the main phase of flux emergence and the jet. A "0" means that jets are produced during the main flux-emergence phase. Column 4 notes (with a tick) if flux cancellation below the jets was observed. Column 5 gives the time in hours between jets if more than 2 jets were observed from the same site. Columns 5, 6, and 7 note whether a surge, filament or circular ribbon was observed at the site of the jets. Blanks in the table indicate there was no data and an "X" that there was data but the feature was not present. Where the interpretation of the data was ambiguous there is a question mark. The tabulated features are chosen to distinguish the various scenarios discussed in the review.

2 Interplanetary jets

The signature of interplanetary jets is a D-H (frequency 10–0.1 MHz) radio type III burst. Type III bursts are produced when sub-relativistic electron beams propagate from the Sun through interplanetary space. They produce bright bursts of radio emission that rapidly drift from above 10 to 0.1 MHz as a function of time (see, Reid & Ratcliffe (2014) and references therein). The drift speed depends on the exciter beam and the density decrease in surrounding plasma. The sub-relativistic, 0.02c–0.35c, electron beam (Dulk et al. 1987; Krupar et al. 2015) excites Langmuir waves with a frequency proportional to the square root of the electron density. The radio brightness depends on both the energy of the electrons and their flux (Dulk et al. 1998). Interplanetary jets originate from open flux regions in the vicinity of active regions (Klein et al. 2008). As well as 2–120 keV electrons (Benz et al. 2001; Klassen et al. 2011; Krucker et al. 1999; Reames et al. 1985), interplanetary jets also accelerate ions (0.3 to 4 MeV amu^{-1}). These ions are characterised by dramatically enhanced (up to 10^4) ^{3}He/^{4}He abundances (Nitta et al. 2006; Pick et al. 2006; Reames & Stone 1986; Wang et al. 2006b) and moderately enhanced (up to 100) heavy ion abundances compared with the standard solar wind. Within active regions, interplanetary jets have been seen from the edge of sunspot umbra, the edge of the penumbra, plage and/or small active region coronal holes.

2.1 Sunspot

Series of jets have been observed on the edge of sunspot umbrae (Innes et al. 2011; Nitta et al. 2008). Innes et al. (2011) made a detailed analysis of a series of six interplanetary jets seen in 2.5 hours (Fig. 1) and concluded that the jets were not triggered by flux emergence because no flux emergence was visible and there were no cold plasma surges alongside the the hot jets. The trigger may have been related to sunspot waves (Chandra et al. 2015; Sych et al. 2015) forcing reconnection between the sunspot open flux and closed field connected to opposite polarity satellite flux. ^{3}He-rich 0.4–1 MeV nucleon^{-1} ions and 40–200 keV electrons have also been detected from a sunspot jet (Nitta et al. 2008).

2.2 Moving magnetic features

Strong interplanetary jets are frequently seen from the region just beyond sunspot penumbrae or pores (Chifor et al. 2008) where minor polarity satellite or moving magnetic feature (MMF) flux reconnects with concentrations of main

Table 1 Characteristics of X-ray/EUV jets. A description of the column entries is given in the text at the end of Sect. 1.

Jet Type	SEPs	Emerge (h)	Cancel	Multiple (h)	Surge	Filament	Circular Ribbon	Reference
IP (SS)	^{3}He			6–12				Nitta et al. 2008
IP (SS)		X		0.3–0.5	X	X	X	Innes et al. 2011
IP (MMF)			✓	0.5–1.0	✓			Chifor et al. 2008
IP (MMF)			✓		✓			Chen et al. 2013
IP (MMF)					✓	✓		Li et al. 2015
IP (MMF)		1–2	✓	0.5–3.5	✓			Chandra et al. 2015
IP (MMF)			✓	0.5–2.0	✓			This work – 2012 July 02
IP (Plage)	^{3}He	36			✓	✓	✓	Bučík et al. 2015
IP (Plage)		24–48	?		✓			Schmieder et al. 2013
IP (ARCH)	^{3}He	24						Wang et al. 2006a
IP (ARCH)		48	✓		✓	✓		Liu et al. 2011
IP (ARCH)					X	X		Alissandrakis et al. 2015
IP (ARCH)	^{3}He	36		18	✓	✓	✓	Bučík et al. 2015
IP (ARCH)	^{3}He	60			✓	✓	✓	This work – 2014 May 16
C (MMF)		0		1–2	✓			Cheung et al. 2015
C (MMF)		X	✓	1–2	✓			Chen et al. 2015
C (Plage)		24–48	?	0.5–0.7	✓			Guo et al. 2013
C (ARCH)				0.5–1	✓		✓	Zhang & Ji 2014
C (PCH)					✓			Cirtain et al. 2007
C (PCH)					✓			Patsourakos et al. 2008
C (PCH)					✓			Nisticò et al. 2009
C (PCH)					✓			Moore et al. 2010
C (PCH)			✓		✓			Young & Muglach 2014
C (PCH)					✓	✓		Sterling et al. 2015
C (ECH)		3	✓	>1				Yang et al. 2011
C (ECH)		6	✓				✓	Huang et al. 2012
C (ECH)					✓		✓	Chandrashekhar et al. 2014
C (QS)			✓	X	✓	✓		Hong et al. 2011
C (QS)		X	✓	X	✓			Innes et al. 2010
C (QS)		X	✓	X	✓	✓	✓	Adams et al. 2014

polarity flux. The cause of MMFs on the edge of sunspots is not fully understood (Hagenaar & Shine 2005; Rempel 2015; Thomas et al. 2002). Analysis of sunspot simulations led Rempel (2015) to suggest that they result from a magneto-convection process related to the strength of the canopy field beyond the penumbra.

At the time of writing, there were no recent good examples in the literature of jets from sunspot MMFs, but it is easy to find plenty of examples by browsing the SDO (Lemen et al. 2012; Scherrer et al. 2012) data with jhelioviewer [1]. A typical example from 2012 July 02 is illustrated in Fig. 2. Here the SDO/AIA 94 Å images of four strong jets have been superimposed on the SDO/HMI longitudinal magnetic field. The WAVES radio data for the time period of the EUV jets are shown in Fig. 3(a). In the figure underneath the 94 Å light curve from the jet region is plotted together with the integrated 1–10 MHz radio emission. There were seven interplanetary EUV jets in 7 hours. As can be seen in the online movie (120702_jets), most jets do not occur when the flux emerges but from the slowly disappearing, and outward moving minor polarity (positive) fields. Once the minor polarity flux disappeared, the jets stopped. Later in the day, more positive flux appeared at the same site. Flux cancellation produced a series of coronal jets (Chen et al. 2015). Although not shown all these jets were also associated with surges seen in 304 Å. Canfield et al. (1996) described X-ray jets associated with Hα surges overlying MMFs before the availability of WAVES data. It is possible that these were also interplanetary jets. The cold plasma may be ejected as a result of flux emergence or it may be filament material that has formed during the evolution of the sunspot surroundings. We note that interplanetary jets from MMFs and SSs are frequently seen in groups of more than three with an interval of 20 min to a couple of hours between jets implying a relatively short energy buildup time.

[1] See www.jhelioviewer.org

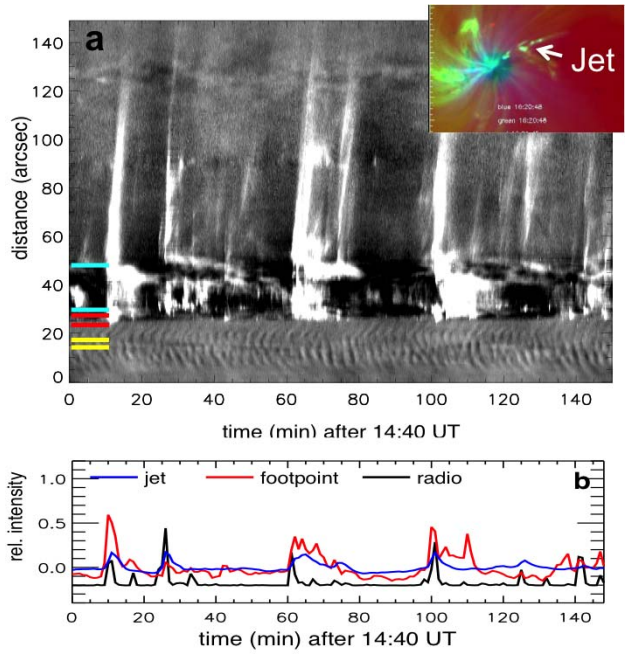

Fig. 1 Jets on the edge of a sunspot (Innes et al. 2011). (*a*) Time series of AIA 211 Å intensity along the jet. On the left the red and blue lines indicate the loop footpoint and loop regions and the yellow lines are centred on the sunspot umbra. The inset shows a three color composite of line-of-sight magnetic field (red), 304 Å (blue) and 211 Å (green) at the time of the jet at 16:20 UT (100 min) on 2010 Aug 3. (*b*) Light curves of 1–10 MHz radio (black), and 211 Å footpoint (red) and jet (blue) emissions.

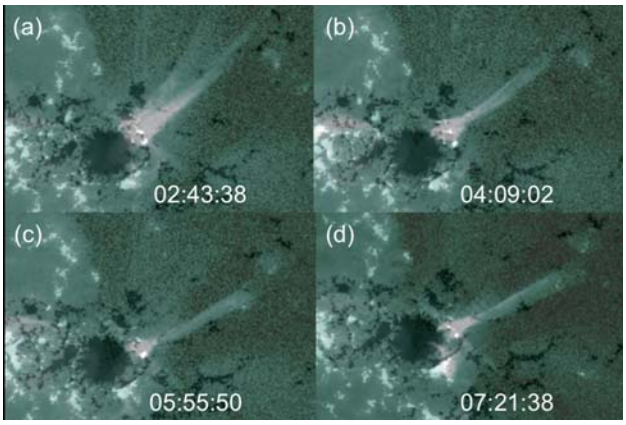

Fig. 2 SDO AIA 94 Å images superimposed on the HMI longitudinal magnetic field for four interplanetary jets seen between 00:00 and 12:00 on 2012 July 02. A movie of the jets and MMFs is online.

2.3 Unipolar plage and active region coronal holes

The bright chromospheric emission close to and inside active regions is known as plage. The underlying magnetic fields are stronger than quiet Sun and often unipolar reflecting their origin which is either dispersed sunspot or recently emerged active region field (Borrero et al. 2015). They may develop into active region coronal holes (ARCHs) which are regions of open field with low coronal emission close to active regions. In both plage and ARCHs magnetic fields concentrate along supergranular boundaries. Flux emergence is followed by at least 24 hours before a strong interplanetary jet is ejected. Post-jet loops often form a small circular patch of EUV loops with a broken ring of chromospheric ribbons at their footpoints.

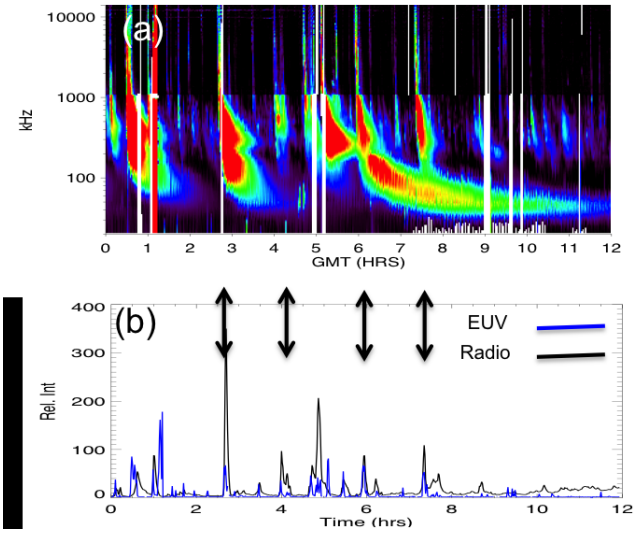

Fig. 3 Radio D-H type III bursts associated with jets from sunspot MMF on 2012 July 2: (*a*) WIND/WAVES radio spectra; (*b*) light curve of 94 Å emission (EUV) and integrated 1–10 MHz radio flux. The double headed arrows mark emission from jets shown in Fig. 2.

Interplanetary jets from ARCHs may be recurring (Bučík et al. 2014; Wang et al. 2006b) or single jets (Liu et al. 2011). Some are associated with filament eruption (Liu et al. 2011) but not all (Alissandrakis et al. 2015). Liu et al. (2011) suggest that flux emergence triggered the jet that they analysed but inspection of the long-time evolution shows that flux emergence occurred 48 hours before the jet. Subsequently a filament formed along the neutral line between the emerged flux and coronal hole field. This was ejected with the jet.

One of the plage jets and several of the ARCH jets were sources of ^{3}He-rich solar energetic particles. One of the best examples, observed on 2014 May 16, was reported by Nitta et al. (2015). It produced a ^{3}He/^{4}He enhancement of about $5{\times}10^4$ over that measured in the fast wind. The interplanetary signatures (type III radio burst, SEPs with dispersive onset) of the jet, shown in Fig. 4, are typical of the other ^{3}He jets in Table 1. A few snapshots of the magnetic field, the chromospheric (304 Å) and coronal (193 Å) plasma from the time of flux emergence to the jet are shown in Fig. 5. When the flux emerges, reconnection rapidly occurs between the minor polarity (negative in this case) and the surrounding major polarity flux, creating a series of radial loops connecting the minor polarity to the surrounding flux. A series of further small jets and brightenings were seen over a few days. Gradually a small, almost circular filament formed along the neutral line encircling the minor polarity.

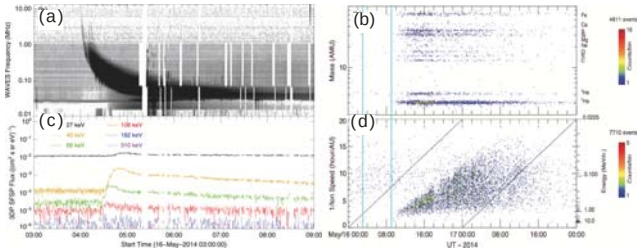

Fig. 4 ACE interplanetary signatures of jet on 2014 May 16 (Nitta et al. 2015): (*a*) WAVES radio dynamic spectrum; (*b*) mass spectrograms in energy range 0.4–10 MeV nucleon^{-1}; (*c*) 3DP Electron fluxes; (*d*) 1/ion speed for ions with mass between 10–70 AMU.

Similar circular filaments were also seen before flares producing circular Hα ribbons (Wang & Liu 2012). The configuration is similar to the polar jet model of Pariat et al. (2009) except here a filament forms along the neutral line. We note that during flux emergence no interplanetary jet was produced; however flux emergence inside the unipolar region was necessary to produce the embedded minor polarity and thus create the field structure suitable for interplanetary jet production.

The eruption occurred sequentially with filament sections lifting off one after another. If viewed from the correct angle and at the right time, helical structure in the cold plasma can be seen (Fig. 6c).

In all studied plage and ARCH cases in Table 1, flux emergence was observed 1–3 days before the jet. Unlike the SS and MMF jets, multiple jets are rare reflecting a longer buildup time for these types of jets. Filament eruption was seen in four cases. Since there was one case where no filament was seen, filament formation is not necessary for jet production. The filament may form as a consequence of flux cancellation and shearing along the neutral line surrounding the minor polarity, as proposed by van Ballegooijen & Martens (1989). The filament then erupts at the time of the jet that started from the onset of an instability in the stressed configuration (Pariat et al. 2009).

3 Coronal jets

Coronal jets are seen to extend into the corona in X-ray and EUV images but do not produce D-H type III radio emission. Examples are X-ray jets from polar and equatorial coronal holes (Cirtain et al. 2007; Moore et al. 2010; Subramanian et al. 2008) where the photospheric magnetic fields are typically quiet Sun values (< 100 G). They also occur at the base of closed active region loops (Cheung et al. 2015; Lee et al. 2013; Strong et al. 1992). Some produce metric U-type radio bursts (Aurass et al. 1994; Karlicky et al. 1996) implying propagation of sub-relativistic electrons in coronal loops.

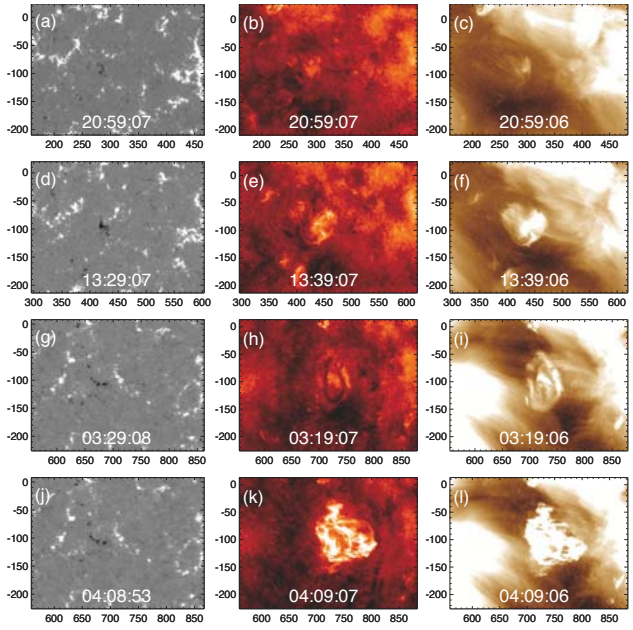

Fig. 5 Magnetic field (scaled between ±250 G) and EUV images of the ARCH jet on 2014 May 16: (*left*) magnetic field; (*middle*) AIA 304 Å; (*right*) AIA 193 Å. Dates are top row 2014 May 13, second row 2014 May 14, third and fourth rows 2014 May 16.

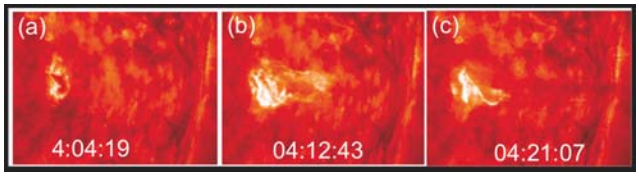

Fig. 6 EUV (304 Å) images of the ARCH jet evolution on 2014 May 16: (*left*) pre-jet; (*middle*) onset; (*right*) helical structure.

3.1 Active regions

Many active region jets do not produce interplanetary signatures either because they occur in closed-field regions or because they are too weak. For example, Li et al. (2012) counted 575 jets from a recently emerged active region over 12 days but less than 10 % were associated with type IIIs. Like the interplanetary jets they generally have both hot and cold components which are not fully intermingled. Spectroscopic observations of the cold component sometimes show evidence for twist (Cheung et al. 2015). This may indicate recent flux emergence (Cheung et al. 2015), the twisting of a fan-spine structure (Wyper & DeVore 2015), or reconnection driven by MMFs. Not all active region coronal jets are twisted (Chen & Innes 2016). Future analysis of IRIS (De Pontieu et al. 2014) and SDO data should be able to sort out the relationship between the hot and cold components and whether the jets appear with flux emergence and/or energy and currents are built up in the corona by footpoint motions (Guo et al. 2013).

3.2 Coronal holes

The polar coronal holes and their equatorward extensions are the source of many X-ray and EUV jets. Coronal holes rotate quasi-rigidly forced by the rigid rotation of the outer corona to which they are connected. This causes a buildup of current between the rigidly rotating open coronal flux and differentially rotating photospheric flux. It has been suggested that field lines continually reconnect leading to a high rate of EUV and X-ray jets and brightenings along the boundary of coronal holes (Sako et al. 2013; Subramanian et al. 2008; Yang et al. 2011).

3.2.1 Polar

X-ray and EUV jets from the polar coronal holes are often projected against the corona which allows one to see faint fast features and their continuation in white-light coronagraph images (Moore et al. 2015; Nisticò et al. 2009; Wang et al. 1998a). The plane-of-sky speeds of polar coronal hole X-ray jets ranges up to 800 km s^{-1}, the Alfvén speed in the lower corona, with an average speed of about 200 km s^{-1} (Cirtain et al. 2007). Because the EUV background is low, faint features at the jet origin can also be identified. As with the active region jets, one frequently observes hot and cold components that appear to follow different paths (Moore et al. 2013). Recently it has been suggested by Sterling et al. (2015) that all polar jets start with a filament eruption because in all the edge-on jets that they studied in polar coronal holes, a filament rises close to the base of the jet before footpoint brightening or jets in X-ray and hot channel EUV emission are seen. As suggested in Sect. 2.3, the filament may be a common bi-product of reconnection along a sheared neutral line that erupts with the jet, but it is not necessarily vital for eruption.

Pariat et al. (2009, 2015) have suggested a model for coronal hole jets that assumes a minor polarity flux concentration in a unipolar field. The minor polarity connects to the dominant flux in all directions creating a circular fan of loops, as seen Fig. 5(f) and (i). Sub-surface flows may then wind up the field, increasing its internal stress until it reaches a critical value and erupts. There is no filament in this model, so the eruption is caused by the opening of the coronal field not by a filament forcing the field opening. It would be interesting to see if including a filament in the model would change the initiation process.

Support for the field opening scenario is provided by a unique series of STEREO (Howard et al. 2008) quadrature observations of a quiet Sun eruption taken with STEREO-A observing at high cadence (2.5 min) in 171 Å and, simultaneously, STEREO-B in 304 Å (Innes et al. 2010). Thus response of the corona seen on the disk could be precisely compared to the cold-plasma eruptions on the limb (Figs. 7 and 8). Analysis of both quiet Sun and coronal hole events showed that the filament rise is nearly always preceded by dimming in the corona which implies that the eruption starts

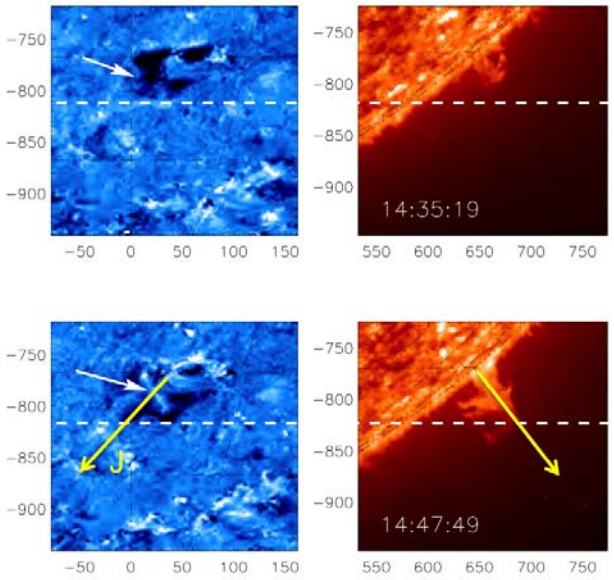

Fig. 7 STEREO-A 171 Å base difference, and simultaneous STEREO-B 304 Å intensity images of a quiet Sun eruption: onset (*top row*), beginning of the fall back (*bottom row*). The yellow arrows in the bottom two images indicate the line along which the time series in Fig. 8 are taken.

with field opening and is followed by filament rise and footpoint brightening.

Other models, for example Moore et al. (2010), Raouafi et al. (2010), and Sterling et al. (2015), propose a linear, arch-like, configuration with a loop connecting the minority polarity and the coronal hole field in one direction, with a possibly sigmoid-shaped progenitor. This linear configuration would be more likely if the original coronal hole flux is not uniformly distributed. Whether the reconnection occurs from arch-like or fan-like loops probably depends on the flux distribution in the plage/coronal hole surrounding the emerging flux. Unfortunately, projection usually obscures, the magnetic field and chromospheric structure at the poles so it is difficult to verify if the structure at the base of these jets is linear, as proposed by Moore et al. (2013) or fan-like as proposed by Pariat et al. (2009).

Another common feature of large polar coronal hole jets is helical structure in the cold plasma (304 Å) emission (Moore et al. 2015, 2013; Patsourakos et al. 2008; Shen et al. 2011). The helical structure is explained as untwisting due to Alfvén waves generated during magnetic energy release of an untwisting loop system or filament (Canfield et al. 1996; Pariat et al. 2009; Raouafi et al. 2010). An alternative explanation, demonstrated in Fig. 6(c), is that sequential reconnection above a circular filament creates what looks like an untwisting structure.

3.2.2 Equatorial

Equatorial coronal holes allow the study of the jets' magnetic environment and footpoint structure (Chandrashekhar

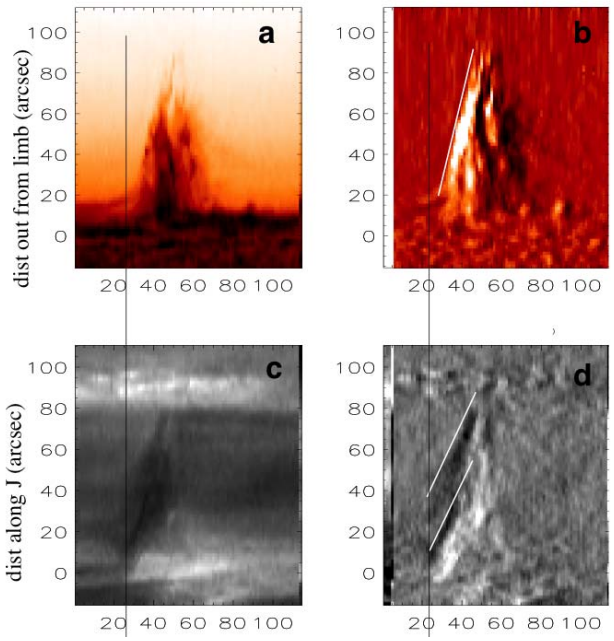

Fig. 8 304 Å and 171 Å time series. (a) and (b) STEREO-B 304 Å along the yellow arrow in bottom right frame of Fig. 7: (*a*) intensity (negative); (*b*) running difference. (*c*) and (*d*) simultaneous STEREO-A 171 Å along the yellow arrow in the bottom left image: (*c*) base difference; (*d*) running difference. The black vertical lines indicate the start time of the eruption seen in 171 Å.

et al. 2014; Huang et al. 2012). Huang et al. (2012) found that jets and brightenings are the result of magnetic flux cancellation about 6 hours after flux emergence. Brightening in and along the coronal hole boundaries is seen more frequently than in the quiet Sun (Subramanian et al. 2010) suggesting that either the open field structure is more conducive to reconnection, the brightenings are more visible due to lower background emission, or the flux emergence rate is different in the two regions. Understandably, many more of the brightenings (70 %) are jet-like compared to the quiet Sun (30 %). There are also about 4–5 times more transition region jets along coronal hole boundaries than in the quiet Sun (Madjarska et al. 2004).

The large number of obvious outflow events along the boundaries has reinforced the suggestion that coronal hole boundary outflows contribute significantly to the slow solar wind (Madjarska et al. 2004; Wang et al. 1998b; Woo et al. 2004).

4 Quiet Sun

In the quiet Sun, supergranule flows cause entrained concentrations of magnetic flux to accumulate at cell junctions. Here vortex-like flows may twist the field leading to current buildup and eruption (Innes et al. 2009). As shown in Fig. 9 quiet Sun X-ray brightenings and small-scale eruptions occur at the junctions of supergranular cells where vortices entwine opposite polarity flux concentrations (Attie et al.

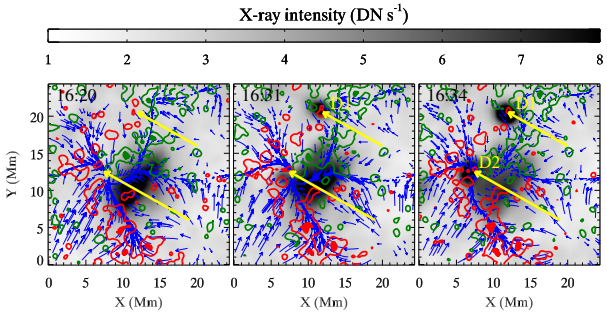

Fig. 9 Snapshots of quiet Sun X-ray brightening (Attie et al. 2016). X-ray images (gray color table) and contours of magnetograms. Red/green (respectively) is positive/negative polarity. Filled contours at +/-40 G, thin contours at +/-10 G. The blue arrows are the velocity vectors to show the direction of the flow. Their length is scaled linearly with the magnitude of the flow. The yellow arrows point at the location of the X-ray transients.

2016; Innes et al. 2009; Innes & Teriaca 2013). Like the coronal hole jets reported by Sterling et al. (2015) these eruptions also often have a filament at their core (Adams et al. 2014). The jet-like nature of the eruptions has been revealed by spectroscopic observations (Innes & Teriaca 2013).

5 Summary

We have categorised jets reported in the literature. Jets associated with sub-relativistic electrons capable of producing type III D-H radio bursts (interplanetary) have been observed (i) on the edge of sunspot umbra, (ii) just beyond the penumbra where there are opposite polarity moving magnetic features (MMF), (iii) from plage, and (iv) from active region coronal holes (ARCH). ^{3}He-rich SEPs were detected from jets at the edge of sunspot umbra, plage and ARCH. So far there have been no specific reports of ^{3}He from MMF jets but that is probably because MMFs are hard to see when the sunspots are at the nominal spacecraft connection point (about 55°W). Because no polar coronal hole jet, not even the strongest observed, have produced type III bursts, it is likely that not enough sub-relativistic electrons are produced in polar coronal hole jets. We speculate that it is related to the weaker photospheric magnetic field strength.

Jets result from magnetic reconnection during (i) flux emergence, (ii) on the edge of sunspot umbrae possibly forced by sunspot waves, (iii) between opposite polarity MMFs, driven by sub-surface outflows from the sunspot, (iv) the winding up of spine-fan fields in unipolar flux regions, (v) at the junctions of supergranular cells where mixed polarity flux is entwined in vortex-like flows, and (vi) along the boarders of coronal holes forced by the different rotation speeds of the open and photospheric fluxes. Interplanetary jets from sunspots and MMFs have a signif-

icantly higher repetition rate than those from unipolar regions where a longer buildup phase seems to be required.

Four types of trigger have been proposed: (i) flux emergence, (ii) filament rise, (iii) opening of coronal field and, (iv) reconnection driven by footpoint motions. Most observational analyses favour the filament eruption. We found one recent paper where flux emergence was considered to be directly responsible for the observed jets and one that reported evidence for coronal field opening. Interestingly recent simulations have concentrated on the flux emergence and coronal field opening rather than reconnection driven by footpoint motion.

Future observations, particularly of the photospheric magnetic field during the jet buildup phase, and from more than one viewing angle are needed to understand the triggering mechanism. Spectroscopic observations can give more complete information on flow motions and twist along jets. Also studies of SEP abundances compared to the source type and buildup time could lead to important information on the SEP acceleration process at reconnection sites.

Acknowledgements. We thank the referee for the constructive comments. R.B. was supported by DFG grant BU 3115/2-1.

References

Adams, M., Sterling, A. C., Moore, R. L., & Gary, G. A. 2014, ApJ, 783, 11
Alexander, D., & Fletcher, L. 1999, Sol. Phys., 190, 167
Alissandrakis, C. E., Nindos, A., Patsourakos, S., Kontogeorgos, A., & Tsitsipis, P. 2015, A&A, 582, A52
Attie, N.-H., Innes, D. E., Solanki, S. K., & Glassmeier, K. H. 2016, A&A, submitted
Aurass, H., Klein, K.-L., & Martens, P. C. H. 1994, Sol. Phys., 155, 203
Bain, H. M., & Fletcher, L. 2009, A&A, 508, 1443
Benz, A. O., Lin, R. P., Sheiner, O. A., Krucker, S., & Fainberg, J. 2001, Sol. Phys., 203, 131
Borrero, J. M., Jafarzadeh, S., Schüssler, M., & Solanki, S. K. 2015, ArXiv e-prints
Bougeret, J., Kaiser, M. L., Kellogg, P. J., et al. 1995, Space Science Reviews, 71, 231
Bučík, R., Innes, D. E., Chen, N. H., et al. 2015, Journal of Physics Conference Series, 642, 012002
Bučík, R., Innes, D. E., Mall, U., et al. 2014, ApJ, 786, 71
Canfield, R. C., Reardon, K. P., Leka, K. D., et al. 1996, ApJ, 464, 1016
Chae, J., Qiu, J., Wang, H., & Goode, P. R. 1999, ApJ, 513, L75
Chandra, R., Gupta, G. R., Mulay, S., & Tripathi, D. 2015, MNRAS, 446, 3741
Chandrashekhar, K., Morton, R. J., Banerjee, D., & Gupta, G. R. 2014, A&A, 562, A98
Chen, J., Su, J., Yin, Z., et al. 2015, ApJ, 815, 71
Chen, N., Ip, W.-H., & Innes, D. 2013, ApJ, 769, 96
Chen, N.-H., & Innes, D. E. 2016, ApJ, in prep.
Cheung, M. C. M., De Pontieu, B., Tarbell, T. D., et al. 2015, ApJ, 801, 83
Chifor, C., Isobe, H., Mason, H. E., et al. 2008, A&A, 491, 279
Cirtain, J. W., Golub, L., Lundquist, L., et al. 2007, Science, 318, 1580
De Pontieu, B., Title, A. M., Lemen, J. R., et al. 2014, Sol. Phys., 289, 2733
Dulk, G. A., Goldman, M. V., Steinberg, J. L., & Hoang, S. 1987, A&A, 173, 366
Dulk, G. A., Leblanc, Y., Robinson, P. A., Bougeret, J.-L., & Lin, R. P. 1998, J. Geophys. Res., 103, 17223
Glesener, L., Krucker, S., & Lin, R. P. 2012, ApJ, 754, 9
Guo, Y., Démoulin, P., Schmieder, B., et al. 2013, A&A, 555, A19
Hagenaar, H. J. & Shine, R. A. 2005, ApJ, 635, 659
Hong, J., Jiang, Y., Zheng, R., et al. 2011, ApJ, 738, L20
Howard, R. A., Moses, J. D., Vourlidas, A., et al. 2008, Space Science Reviews, 136, 67
Huang, Z., Madjarska, M. S., Doyle, J. G., & Lamb, D. A. 2012, A&A, 548, A62
Innes, D., McIntosh, S., & Pietarila, A. 2010, A&A, 517, L7
Innes, D. E., Cameron, R. H., & Solanki, S. K. 2011, A&A, 531, L13
Innes, D. E., Genetelli, A., Attie, R., & Potts, H. E. 2009, A&A, 495, 319
Innes, D. E., & Teriaca, L. 2013, Sol. Phys., 282, 453
Kahler, S. W., & Hudson, H. S. 2002, ApJ, 574, 467
Karlicky, M., Mann, G., & Aurass, H. 1996, A&A, 314, 303
Klassen, A., Gómez-Herrero, R., & Heber, B. 2011, Sol. Phys., 273, 413
Klein, K.-L., Krucker, S., Lointier, G., & Kerdraon, A. 2008, A&A, 486, 589
Kosugi, T., Matsuzaki, K., Sakao, T., et al. 2007, Sol. Phys., 118
Krucker, S., Kontar, E. P., Christe, S., Glesener, L., & Lin, R. P. 2011, ApJ, 742, 82
Krucker, S., Larson, D. E., Lin, R. P., & Thompson, B. J. 1999, ApJ, 519, 864
Krupar, V., Kontar, E. P., Soucek, J., et al. 2015, A&A, 580, A137
Kundu, M. R., Raulin, J. P., Nitta, N., et al. 1995, ApJ, 447, L135
Lee, K.-S., Innes, D. E., Moon, Y.-J., et al. 2013, ApJ, 766, 1
Lemen, J. R., Title, A. M., Akin, D. J., et al. 2012, Sol. Phys., 275, 17
Li, L. P., Zhang, J., Li, T., Yang, S. H., & Zhang, Y. Z. 2012, A&A, 539, A7
Li, X., Yang, S., Chen, H., Li, T., & Zhang, J. 2015, ApJ, 814, L13
Liu, C., Deng, N., Liu, R., et al. 2011, ApJ, 735, L18
Madjarska, M. S., Doyle, J. G., & van Driel-Gesztelyi, L. 2004, ApJ, 603, L57
Moore, R. L., Cirtain, J. W., Sterling, A. C., & Falconer, D. A. 2010, ApJ, 720, 757
Moore, R. L., Sterling, A. C., & Falconer, D. A. 2015, ApJ, 806, 11
Moore, R. L., Sterling, A. C., Falconer, D. A., & Robe, D. 2013, ApJ, 769, 134
Moreno-Insertis, F., & Galsgaard, K. 2013, ApJ, 771, 20
Moreno-Insertis, F., Galsgaard, K., & Ugarte-Urra, I. 2008, ApJ, 673, L211
Nisticò, G., Bothmer, V., Patsourakos, S., & Zimbardo, G. 2009, Sol. Phys., 259, 87
Nitta, N. 1997, ApJ, 491, 402
Nitta, N. V., Mason, G. M., Wang, L., Cohen, C. M. S., & Wiedenbeck, M. E. 2015, ApJ, 806, 235
Nitta, N. V., Mason, G. M., Wiedenbeck, M. E., et al. 2008, ApJ, 675, L125
Nitta, N. V., Reames, D. V., De Rosa, M. L., et al. 2006, ApJ, 650, 438
Pariat, E., Antiochos, S. K., & DeVore, C. R. 2009, ApJ, 691, 61

Pariat, E., Dalmasse, K., DeVore, C. R., Antiochos, S. K., & Karpen, J. T. 2015, A&A, 573, A130
Patsourakos, S., Pariat, E., Vourlidas, A., Antiochos, S. K., & Wuelser, J. P. 2008, ApJ, 680, L73
Pick, M., Mason, G. M., Wang, Y.-M., Tan, C., & Wang, L. 2006, ApJ, 648, 1247
Raouafi, N.-E., Georgoulis, M. K., Rust, D. M., & Bernasconi, P. N. 2010, ApJ, 718, 981
Raulin, J. P., Kundu, M. R., Hudson, H. S., Nitta, N., & Raoult, A. 1996, A&A, 306, 299
Reames, D. V., & Stone, R. G. 1986, ApJ, 308, 902
Reames, D. V., von Rosenvinge, T. T., & Lin, R. P. 1985, ApJ, 292, 716
Reid, H. A. S., & Ratcliffe, H. 2014, Research in Astronomy and Astrophysics, 14, 773
Rempel, M. 2015, ApJ, 814, 125
Sako, N., Shimojo, M., Watanabe, T., & Sekii, T. 2013, ApJ, 775, 22
Scherrer, P. H., Schou, J., Bush, R. I., et al. 2012, Sol. Phys., 275, 207
Schmieder, B., Guo, Y., Moreno-Insertis, F., et al. 2013, A&A, 559, A1
Shen, Y., Liu, Y., Su, J., & Ibrahim, A. 2011, ApJ, 735, L43
Shibata, K., Ishido, Y., Acton, L. W., et al. 1992, PASJ, 44, L173
Shimojo, M., Hashimoto, S., Shibata, K., et al. 1996, PASJ, 48, 123
Shimojo, M., Shibata, K., & Harvey, K. L. 1998, Sol. Phys., 178, 379
Sterling, A. C., Moore, R. L., Falconer, D. A., & Adams, M. 2015, Nature, 523, 437
Strong, K. T., Harvey, K., Hirayama, T., et al. 1992, PASJ, 44, L161
Subramanian, S., Madjarska, M. S., & Doyle, J. G. 2010, A&A, 516, A50
Subramanian, S., Madjarska, M. S., Maclean, R. C., Doyle, J. G., & Bewsher, D. 2008, A&A, 488, 323
Sych, R., Karlický, M., Altyntsev, A., Dudík, J., & Kashapova, L. 2015, A&A, 577, A43
Thomas, J. H., Weiss, N. O., Tobias, S. M., & Brummell, N. H. 2002, Nature, 420, 390
Török, T., Aulanier, G., Schmieder, B., Reeves, K. K., & Golub, L. 2009, ApJ, 704, 485
Tsuneta, S., Acton, L., Bruner, M., et al. 1991, Sol. Phys., 136, 37
van Ballegooijen, A. A., & Martens, P. C. H. 1989, ApJ, 343, 971
Wang, H., & Liu, C. 2012, ApJ, 760, 101
Wang, T. J., Innes, D. E., & Solanki, S. K. 2006a, A&A, 455, 1105
Wang, Y., Pick, M., & Mason, G. M. 2006b, ApJ, 639, 495
Wang, Y.-M., & Sheeley, Jr., N. R. 1993, ApJ, 414, 916
Wang, Y.-M.,, Sheeley, Jr., N. R., Socker, D. G., et al. 1998a, ApJ, 508, 899
Wang, Y.-M., Sheeley, Jr., N. R., Walters, J. H., et al. 1998b, ApJ, 498, L165
Woo, R., Habbal, S. R., & Feldman, U. 2004, ApJ, 612, 1171
Wyper, P. F., & DeVore, C. R. 2015, ArXiv e-prints
Yang, S., Zhang, J., Li, T., & Liu, Y. 2011, ApJ, 732, L7
Young, P. R., & Muglach, K. 2014, Sol. Phys., 289, 3313
Zhang, Q. M., & Ji, H. S. 2014, A&A, 567, A11

